An approach to the retrieval of thin cloud optical depth from a Cimel sun-photometer

J. L. Guerrero-Rascado[1,2,3], M. J. Costa[1,4], A. M. Silva[1,4], F. J. Olmo[2,3]

Abstract — In this work we proposed a technique to retrieve optical depth for optically thin clouds (clouds that enable the transmission of solar radiation through them). This method complements the current performance of AERONET for optically thick cloud measurements using data eliminated by the cloud-screening algorithm that are not useful to derive aerosol properties, therefore inexpensively increasing the capabilities of the sun-photometers. It is based on the computation of apparent cloud optical depths and a forward scattering correction method that exploits state-of-the-art ice cloud scattering models. This complementary procedure is applied to Cimel sun-photometer measurements performed at the Évora Geophysics Centre (Portugal, 38.6ºN, 7.9ºW, 293 m asl) in order to obtain a climatology of optical depths for optically thin clouds over middle-latitude regions. A comparison with MODIS retrievals is presented. Main features regarding annual variability from 2007 to 2010 are also reported.

Keywords — cloud optical depth, sun-photometer, optically thin clouds

1 Introduction

Clouds play an important role in the radiative energy budget of the Earth-atmosphere system and in the hydrological cycle and hence in the Earth's climate system. Particularly, cirrus clouds are widely recognized to play this important role [1], [2]. Some parameters that control the extinction radiative process in a cloudy media (absorption and scattering of radiation) are cloud optical depth, single scattering albedo, phase function, surface albedo and geometrical distribution. A change in almost any aspect of clouds, such as their type, location, water content, cloud altitude, particle size and shape or lifetimes, affects the degree to which clouds warm or cools the Earth. In this sense, considerable effort has been done in order to understand the role of clouds in climate change, but observational evidence is still lacking, particularly regarding how the cloud optical depth responds to climate perturbations [3]. Parallel to the model development, a great effort has been performed to develop a wide dataset of ground-based measurements, not only to provide an adequate reference for satellite observations, but also to make possible an empirical analysis of cloud processes [4]. Therefore, a dramatic increase in both the number and accuracy of cloud optical depth observations is crucial for validation of satellite data, improvement of climate model predictions and understanding cloud-related phenomena.

The well-known Aerosol Robotic Network - AERONET- [5] is a ground-based network based on Cimel sun-photometers, and is designed to obtain optical and microphysical properties of the atmospheric aerosols from sun/sky measurements of spectral radiances. The standardized network procedures of instrument maintenance, calibration, cloud screening and data processing allow for quantitative analysis of the aerosol data obtained in more than 500 globally distributed stations. AERONET products are provided in three categories: a) raw (level 1.0); b) cloud-screened (level 1.5) following the cloud-screening algorithm described by [6]; and c) cloud screened and quality-assured (level 2.0). The AERONET algorithm is based on several criteria; the most important ones are related to temporal variations of aerosol optical depth at short scale time, and hourly and diurnal time periods. For a variety of sites this cloud-screening procedure eliminates from 20% to 50% of the initial data [6], [7]. Therefore, the amount of discarded measurements that are not useful to derive aerosol properties is quite high.

Recently, a new capability, the so-called cloud-mode, has been incorporated to AERONET in order to inexpensively increase the number and accuracy of cloud optical depth measurements [8]. It is based on the use of the instrument during the sleep mode. In the cloud mode, the sun-photometers point directly to the zenith when clouds completely block the sun (and therefore, the sun/sky observations are not appropriate for retrieving aerosol properties), performing zenith radiance measurements. This new

1. *J. L. Guerrero-Rascado, M. J. Costa and A. M. Silva are with the Evora Geophysics Centre, University of Evora, Rua Romão Ramalho, 59, 7000 Evora, Portugal. E-mail: jrascado@uevora.pt , mjcosta@uevora.pt, asilva@uevora.pt*
2. *J. L. Guerrero-Rascado and F. J. Olmo are with the Andalusian Center for Environmental Research (CEAMA), University of Granada – Autonomous Government of Andalusia, Av. del Mediterráneo s/n, 18071 Granada, Spain. Email: rascado@ugr.es, fjolmo@ugr.es*
3. *J. L. Guerrero-Rascado and F. J. Olmo are with the Department of Applied Physics, University of Granada, Fuentenueva s/n, 18071 Granada, Spain. Email: rascado@ugr.es, fjolmo@ugr.es*
4. *M. J. Costa and A. M. Silva are with the Department of Physics, University of Évora, Rua Romão Ramalho 59, 7000 Évora, Portugal. E-mail: mjcosta@uevora.pt, asilva@uevora.pt*

mode allows for an alternative way to observe cloud optical properties on a global scale using the existing AERONET infrastructure; however the current cloud mode observation strategy is biased toward measurements of optically thick clouds.

This work proposes an additional method to retrieve optical depth for thin ice clouds that complements the current performance of AERONET for cloud measurements using data eliminated by the cloud-screening algorithm. Section 2 presents the instrument used in this study. In section 3, we describe the methodology developed to retrieve cloud optical depth that includes the computation of apparent cloud optical depths and the development of a forward scattering correction method, based on state-of-the-art ice cloud scattering models. Section 4 presents some results about the application of this complementary procedure to Cimel sun-photometer observations performed at the Évora Geophysics Centre (Portugal, 38.6°N, 7.9°W, 293 m asl) in order to obtain a climatology of thin cloud optical depths over middle-latitude regions and also to extend the cloud research carried out in this station.

2 INSTRUMENTATION

Spectral solar extinction measurements were acquired by a multiwavelength sun/sky photometer manufactured by Cimel Electronique (France). The Cimel CE-318 is a sun-photometer which makes direct sun measurements at several wavelengths in the range between 340 and 1020 nm with a 1.2° full-field-of-view (FOV), and taking about 8 s to scan all wavelengths using a filter wheel. The acquisition is automatic and the measurement sequence depends on the local solar time and on the value of the optical air mass. Measurements are made at an approximate rate of 15 min with a higher frequency when the Sun is close to the horizon. The instrument also includes protocols for the measurements of sky radiance values in a reduced number of wavelengths using almucantar and principal plane geometries. An electronic test is made on the direct solar beam measurements to check the presence of thick clouds: in case the attenuation is large, measurements are not made. This instrument is the standard sun/sky photometer used in the AERONET network. A whole description can be seen in [5]. Langley and laboratory calibrations are performed following the AERONET procedures.

3 METHODOLOGY

3.1 Apparent cloud optical depth

Total optical depths are obtained from direct sun-photometer measurements data using the Bouguer-Lambert-Beer law as:

$$I_{direct} = \exp\left[-\left(\tau_{ray} + \tau_{gas} + \tau_{aerosol} + \tau_{cloud}\right) A_0\right] \qquad (1)$$

where I_{direct} is the transmittance of direct beam at the air mass A_0, which depends on the solar zenith angle; and τ_{ray}, τ_{gas}, $\tau_{aerosol}$ and τ_{cloud} are the optical depths of Rayleigh scattering, gaseous absorption, aerosol extinction and cloud extinction, respectively, which depend on the wavelength [9], [10]. Under normal atmospheric conditions, Rayleigh and absorption optical depths are relatively fixed with only very minor variations, and are defined following the usual procedure in AERONET [5], [9], [10]. Equation (1) allows for the derivation of $\tau_{aerosol}$ for conditions of cloud-free sky (τ_{cloud}=0). The presence of clouds is determined through the cloud-screening algorithm implemented in AERONET. The main threshold criteria are related to temporal variations of $\tau_{aerosol}$. Thus the triplet stability criterion is applied to short scale variability (1 min) and the smoothness criterion to hourly and diurnal period variations of $\tau_{aerosol}$. A detailed description of all used criteria is given in [6]. The application of this algorithm enables to split the sun-photometric measurements in two categories: (i) cloud-free data that are appropriate for aerosol research, and (ii) cloud-contaminated data that traditionally have been discarded.

For overcast sky, equation (1) provides the contribution of both aerosols and clouds to the transmittance of direct beam ($\tau_{aerosol}$+ τ_{cloud}) after subtracting the Rayleigh optical depth and O_3 and NO_2 absorption optical depth. Furthermore, because the temporal scale of the presence of thin clouds in the field of view of the sensor is of the order of minutes, while the temporal scale of aerosols is normally longer on the order of hours, we estimate $\tau_{aerosol}$ interpolating between the closest aerosol optical depths just before and after the cloudy period. These aerosol optical depths are derived following the normal AERONET protocol under cloud-free conditions. Similar procedure has been used previously to retrieve thin cloud optical depth from a multifilter rotating shadow band radiometer [3]. However, it must be stressed that the τ_{cloud} determined using this procedure is considered to be an apparent optical depth and its accuracy is compromised by contamination of the direct transmission due to the forward scattered radiation within the sensor's field of view. The unwanted scattered radiance results in an overestimation of the cloud transmission, and furthermore, it results in an underestimation of the derived cloud optical depth. To correct for the strong forward scattering of solar radiation into the instrument's field of view, a correction method based on state-of-the-art ice cloud scattering models has been implemented.

3.2 Forward scattering correction

The cloud optical depth may be obtained from the apparent cloud optical depth [11], using a correction

factor, as follows:

$$\tau_{cloud} = \tau_{cloud}^{apparent} \frac{1}{1-\omega_0 \frac{\int_0^{FOV/2} p(\theta)\sin\theta d\theta}{\int_0^{\pi} p(\theta)\sin\theta d\theta}} \quad (2)$$

where ω_0 is the single scattering albedo, $p(\theta)$ is the scattering phase function and θ the scattering angle.

The above correction is based on the knowledge of the phase function for angles lower than half FOV angle, therefore the accuracy of the correction strongly depends on the truthfulness of the scattering model employed. The bulk scattering models adopted here are based on reanalysis of in-situ data from a variety of middle - latitude and tropical ice cloud field experiments [12]. The size distributions are based on 45 size bins (particle size ranges from 2 to 9500 microns) and the ice particle habit distributions vary as a function of maximum dimension. Habits considered in the models include droxtals, plates, hollow and solid columns, 3-D bullet rosettes, and aggregates.

The correction factors K_{FSC}, i.e., the factors multiplying the apparent cloud optical depth in (2), are shown in Fig. 1, for the wavelengths considered, as a function of effective radius. Note that the correction factors moderately vary with the effective radius hence a proper use of (2) requires a priori knowledge of the cloud particle effective radius.

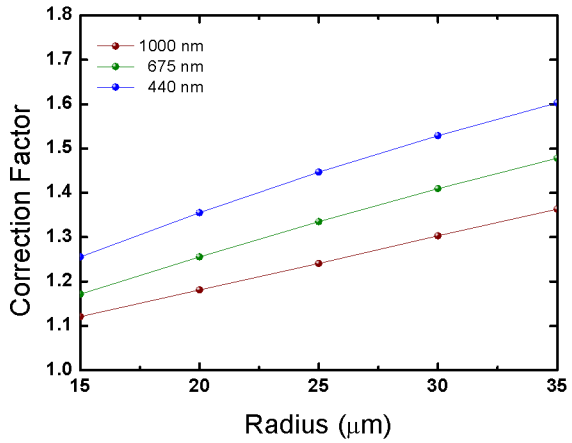

Fig. 1. Correction factors, K_{FSC}, as function of effective radius at several wavelengths.

A two-year (2007-2008) climatology of ice cloud effective radius over Évora was prepared, based on the Moderate Resolution Imaging Spectroradiometer (MODIS) cloud product [13]. Collection 5 of this product is used both from Terra and Aqua satellites and the monthly mean and standard deviation values of the cloud location [14]. In this way, seven distinct possible geographical points are determined as potential pixels to the comparison with Cimel cloud optical depth. Since there is no additional information on cloud base height, at the moment the smallest difference between Cimel and MODIS cloud optical depth, amongst the seven comparisons, is taken.

are shown in Table 1. It can be noted that the mean values do not present a large variation throughout the year, with standard deviations that present the highest values in March and June and the lowest in August and November.

The correction factor is then chosen according to the mean effective radius corresponding to the month being, obtaining thus the real optical thickness (Eq. 2).

Table 1. Monthly mean values of effective radius, r_{eff}, derive from MODIS Terra and MODIS Aqua (period 2007-2008)

Month	r_{eff} (μm)	sd (μm)
January	21.5	8.5
February	24.7	7.6
March	24.0	11.2
April	25.0	7.6
May	25.2	7.8
June	23.7	9.6
July	25.2	-
August	26.7	4.6
September	24.5	6.9
October	24.2	8.0
November	21.9	4.8
December	23.6	7.8

4 RESULTS AND DISCUSSION

4.1 Cimel Sun-photometer versus MODIS

The cloud optical depth retrieved using the aforementioned methodology is compared to the cloud optical depth provided in MODIS cloud product (collection 5), both from Terra and Aqua satellites, for the three-year period, from 2007 to 2009. The different observation geometries of both instruments must be taken into account when co-locating both types of retrievals in order to be in the correct conditions of comparison. The Cimel sun-photometer measures the sun direct radiation (section 2), whereas MODIS is a nadir viewing instrument.

The ice clouds are assumed to have their bottoms located between 6 and 12 km (steps of 1 km) and the corresponding horizontal distances between Évora observatory (where Cimel is installed) and the hypothetical cloud location is then computed. The solar azimuth, the Cimel geographical coordinates and the horizontal distance, are used to estimate the geographical coordinates

Fig. 2 shows the results of the comparison for the three-year period. The greatest dispersion of points is observed for the lower values of cloud optical depth, with the MODIS values considerably higher than those obtained from Cimel. This is not surprising and is consistent with the different observing geometries. Whereas the satellite uses the reflected solar radiation, the sun-photometer measures the transmitted solar radiation. The satellite is thus much less sensitive to very low cloud optical depth values than the Cimel, which is in turn unable to measure high cloud optical thickness values.

Nevertheless, the comparison yields fairly good results, with a high correlation coefficient of 0.96 and an intercept of 0.38, which may be deemed a lowest detection limit of MODIS retrievals.

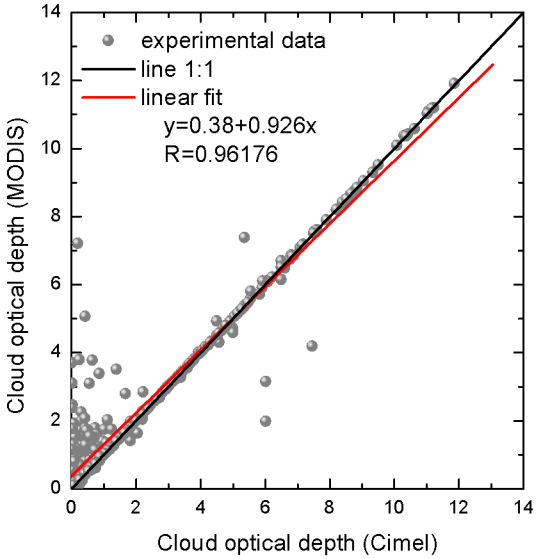

Fig. 2. Comparison of cloud optical depths, $\tau_{cloudFSC}$, derived from sun-photometer and MODIS (period 2007-2009).

4.2 General features

Some basic statistics concerning the whole period 2007–2010 is presented here in order to characterise the cloud optical depths in the region under study.

The performance of a Cimel sun-photometer to derive $\tau_{cloudFSC}$ following the aforementioned procedure is focused on clouds that enable the transmission of solar radiation through the cloudy media and the consequent detection by the instrument. Therefore, cirrus is the main cloud type analyzed here. Traditionally, the cloud research has been classifying cirrus in terms of their optical depths as in subvisual (< 0.03), thin (between 0.03 and 0.3) and dense (> 0.3) cirrus. Following this criterion, we found that ~8% of cirrus clouds are subvisual, 41% of cirrus clouds are optically thin, and 51% of cirrus clouds are dense for all wavelengths except at 675 nm where the values are 6%, 32.9% and 61.1%, respectively (Table 2). A recent study at the Évora station based on 532nm-elastic profiles derived from a Raman lidar indicates similar rates (2% subvisual, 31% thin, 67% dense) at the visible spectral range [15]. Other midlatitude climatologies, such as [16] reported that up to 52% of the cases included in their cirrus climatology analysis are subvisual or thin cirrus using a 694nm-lidar. For the 355nm-wavelength, [17] and [18] found, using Raman lidars that ~71% and up to 60% of the cirrus studied have optical depths below 0.3. Therefore our results are in general agreement with these values.

Table 2. Frequency of presence for several cloud types in terms of optical depth

Channel (nm)	Total	Sub (%)	Thin (%)	Dense (%)
1020	8448	8.7	40.5	50.9
675	14141	6.0	32.9	61.1
440	8723	7.0	41.5	51.5

To better characterize statistically the optical properties of each cloud type, only data fulfilling the classification criteria at all wavelengths simultaneously are considered (7345 cases). The frequency distributions (not shown here), present a different behavior for each cloud type. The frequency distribution of $\tau_{cloudFSC}$ can be well described by a log-normal distribution for thin cirrus (R^2>0.92 at all wavelengths) and by an exponential decay for dense cirrus (R^2>0.97 at all wavelengths). Due to the reduced number of data (around 3%), subvisual cirrus does not present a well defined distribution. The mean, standard deviation, 5% percentile, 25% percentile, median, 75% percentile and 95% percentile are presented in Table 3. Instantaneous $\tau_{cloudFSC}$ were highly variable covering the range from 0.012 (1020 nm) on 3rd November 2007 up to 13.46 (440 nm) on 12th May 2010. Mean values slightly increase as wavelength decrease with linear tendency. At 440 nm, 90% of subvisual cirrus $\tau_{cloudFSC}$ were between 0.016 and 0.029. As it was mentioned in section 3.3, the analysis regarding subvisual cirrus is biased because apparent cloud optical depths below 0.01 are removed from our database. For thin cirrus 90% of $\tau_{cloudFSC}$ data were between 0.04 and 0.27, thus covering almost the entire range of optical depths for such kind of clouds, and for dense cirrus were between 0.37 and 6.98, however most of this percentage is below 3.0 (around 80%) .

Table 3. Basic statistical parameters for $\tau_{cloudFSC}$ for the period of 2007-2010

Cloud type	$\tau_{cloudFSC}$	Mean	Sd	P5	P25	P75	P95	Median
Subvisual	1020	0.021	0.005	0.014	0.017	0.024	0.028	0.021
	675	0.021	0.004	0.015	0.018	0.024	0.027	0.021
	440	0.022	0.004	0.016	0.020	0.025	0.029	0.023
Thin	1020	0.12	0.07	0.04	0.06	0.18	0.26	0.11
	675	0.13	0.07	0.04	0.07	0.18	0.26	0.11
	440	0.14	0.07	0.04	0.07	0.19	0.27	0.12
Dense	1020	1.82	1.93	0.34	0.55	2.31	6.10	1.02
	675	1.91	2.04	0.36	0.58	2.42	6.49	1.07
	440	2.03	2.20	0.37	0.62	2.55	6.98	1.14

4.3 Annual variations

Instantaneous values were used in the calculations of all statistical parameters presented here. Fig. 3 shows the annual mean $\tau_{cloudFSC}$ for each cloud type in order to depict the general behavior at all available wavelengths. Subvisual cirrus did not present a clear trend with mean values between 0.020 and 0.023. In contrast, $\tau_{cloudFSC}$ for thin cirrus experienced at all wavelengths a significant increase, around 9.8%, from 2007 to 2008, and then a slight decrease of 2.0% and 1.3% from 2008 to 2009 and from 2009 to 2010, respectively. For dense cirrus, $\tau_{cloudFSC}$ changes from year to year in a similar way at all wavelengths with increasing and decreasing around 13%. Such variability found for thin and dense cirrus results in modifications on the impact related to the radiative energy redistribution caused by these clouds.

The infrared radiative forcing by cirrus clouds (CRF_{IR}) can be written following the highly simplified relationship given in [19], [20], [21]:

$$CRF_{IR} = k\left(T_{surface}^4 - T_{cloud}^4\right)\cdot\left(1-\exp^{-\frac{D\cdot\tau_{cloudFSC}}{C}}\right) \quad (5)$$

where k is the Stefan-Boltzmann constant (=5.67x10^{-8} Js^{-1}m^{-2}K^{-4}), $T_{surface}$ is the effective surface temperature, T_{cloud} is the cloud temperature, D is the diffusivity factor (=1.66) and C is the constant (=2) relating infrared optical depth to visible optical depth. Assuming identical conditions of temperature along the different years, changes in $\tau_{cloudFSC}$ govern modifications of CRF_{IR}. Thus, forcings of thin cirrus underwent an increase of 9.2% from 2007 to 2008, therefore enhancing the green house effect (warming) caused by this type of clouds. Afterwards, the magnitude of the warming effect decrease slightly around 1.2% and 2.2% from 2008 to 2009 and from 2009 to 2010, respectively.

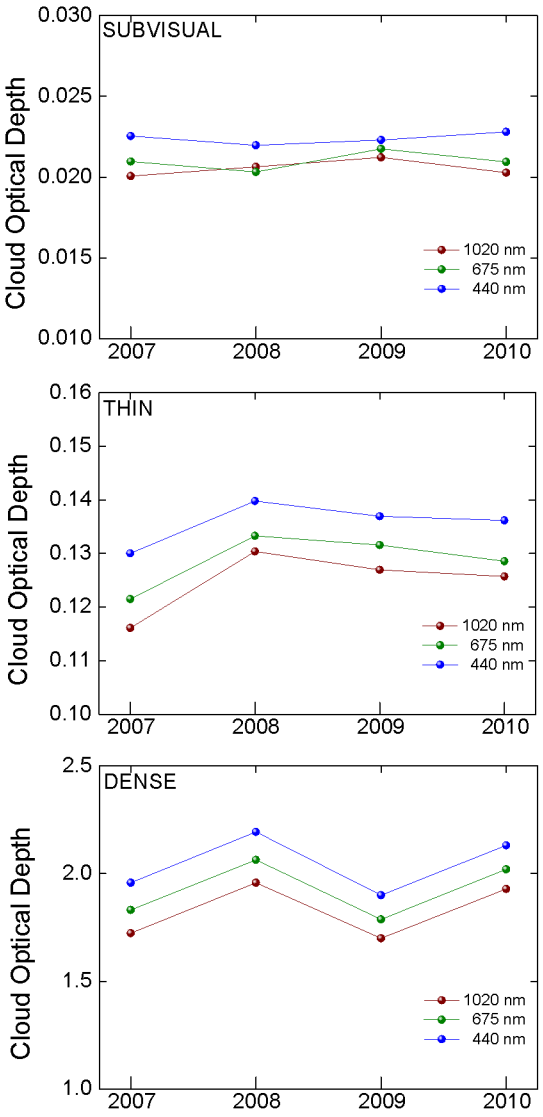

Fig. 3. Annual mean values (period 2007-2010) of cloud optical depth, $\tau_{cloudFSC}$, for subvisual, thin and dense cirrus.

For dense cirrus, forcings presented the same behaviour than $\tau_{cloudFSC}$ with increasing and decreasing around 5.2% from year to year. Therefore, taking as reference the year 2007, we conclude thin cirrus have intensified the warning of the atmosphere although with a slowly reducing tendency, whereas dense cirrus have ranged from year to year with a smaller warming effect.

Instantaneous values of $\tau_{cloudFSC}$ for each wavelength were found to be highly variable, ranging from values close to the detection limit up to 13.46 (at 440 nm). Fig. 4 presents box charts regarding basic statistic at 675 nm in order to better characterize $\tau_{cloudFSC}$ from 2007 to 2010. The mean, 5% percentile, 25% percentile, median, 75% percentile and 95% percentile are shown in this fig.

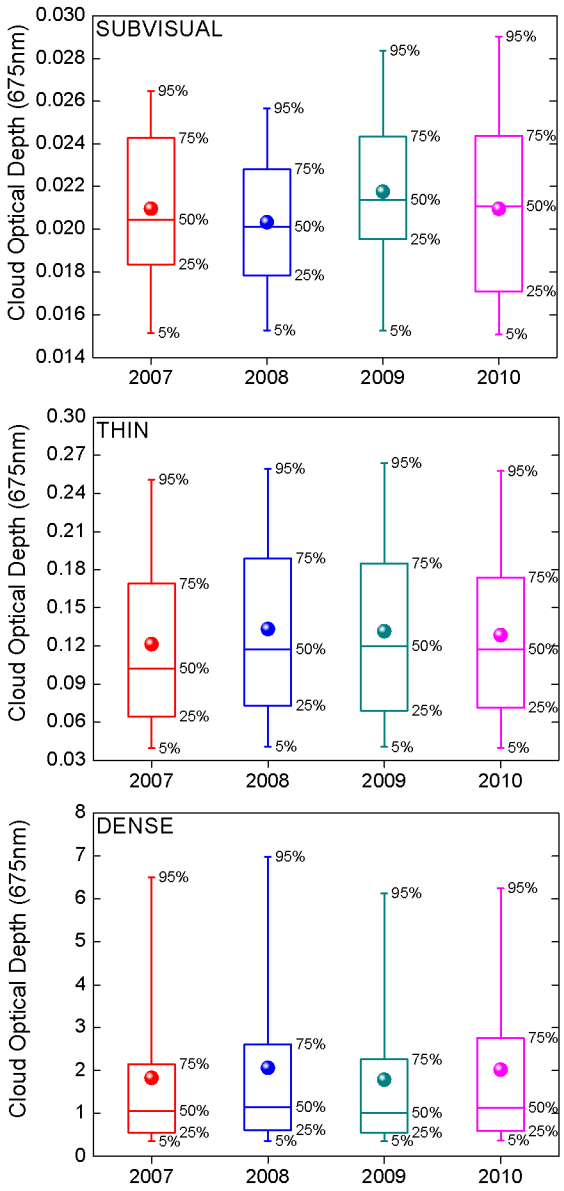

Fig. 4 Annual box charts of cloud optical depth, $\tau_{cloudFSC}$, at 675 nm for subvisual, thin and dense cirrus.

As it was mentioned previously, subvisual cirrus did not present a clear tendency during the selected period and the results for one wavelength cannot be extrapolated to others.

For thin cirrus, 90% of the $\tau_{cloudFSC}$ were in the range of 0.04-0.25 in 2007 and of 0.4-0.26 in the other years, but most of this percentage is below 0.20 (around 80%). In addition, median (and mean) values increased from 0.10 (0.12) in 2007 to 0.12 (0.13) in the other years. Some statistical parameters such as mean, median, 25% percentile, 95% percentile and maximum showed an increase with respect to 2007, indicating larger $\tau_{cloudFSC}$ during the last years.

The $\tau_{cloudFSC}$ values for dense cirrus fit to exponential decay distribution with a long tail, which implies larger differences between mean and median values (around a factor of 1.8) and ranges between 75% percentile and 95% percentile very wide (around a factor of 2.7). Changes at all statistical parameters were observed from year to year following similar tendency to that observed for the other wavelengths (Fig. 3). Around 46-50% and 67-73% of data (depending on the year) are lower than 1.0 and 2.0, respectively, which indicates most of the cirrus even classified as dense cirrus has relatively low $\tau_{cloudFSC}$ and can be labeled as optically thin clouds. The largest variability (in terms of maximum-minimum value) was registered in 2010 with maximum values up to 12.83.

5 Conclusions

We proposed a method for the determination of optical depths in optically thin clouds, exploiting sun-photometer data that are routinely measured and not useful to derive aerosol properties, therefore inexpensively increasing the capabilities of AERONET.

The factors, K_{FSC}, which take into account the forward scattered radiation within the sun-photometer's FOV, allowed for converting the apparent cloud optical depth into real cloud optical depths. These factors moderately vary with the effective radius and two-year climatology of cloud particle effective radius from MODIS was used to increase the accuracy of the correction factors.

From the analysis of $\tau_{cloudFSC}$ over Évora from 2007 to 2010, we conclude that the frequency distribution of $\tau_{cloudFSC}$ is well described by a log-normal distribution for thin cirrus and by an exponential decay for dense cirrus. A clear distribution was not found for subvisual cirrus. We found annual differences among the cloud types studied.

Regarding annual variability, subvisual cirrus did not present a clear trend whereas thin cirrus experienced a significant increase (around 9.8%) from 2007 to 2008, and then a slight decrease (up to

2.0%) during the other years. The consequence was an increment (of similar magnitude) of the green house effect (warming) caused by thin cirrus from 2007 to 2008, although a clear slowly reducing tendency was observed from 2008. Dense cirrus changed from year to year with increments and decrements around 13%, and causing warming effects smaller than those induced by thin cirrus.

The method presented here will potentially increase the knowledge on optical thin clouds benefiting of the long-term and wide global coverage provided by AERONET.

ACKNOWLEDGMENT

This work has been supported by the National Reequiment Programme Rede Nacional de Geofísica REDE/1527/RNG/2007, by the FEDER (Programa Operacional Factores de Competitividade – COMPETE) and by National funding through FCT – Fundação para a Ciência e a Tecnologia in the framework of project FCOMP-01-0124-FEDER-007122 (PTDC / CTE-ATM / 65307 / 2006), by the FCT fellowships SFRH/BPD/63090/2009, by the Spanish Ministry of Education fellowship EX2009-0700 and by the project P08-RNM-3568. The authors thank the MODIS Team for maintaining and providing all necessary information.

REFERENCES

[1] I. Schlimme, A. Macke, and J. Reichardt, "The impact of ice crystal shapes, size distributions, and spatial structures of cirrus clouds on solar radiative fluxes", *J. Atmos. Sci.*, 62, pp. 2274-2283, 2005

[2] J.M. Futyan, J.E. Russell, and J.E. Harries, "Determining cloud forcing by cloud type from geostationary satellite data", *Geophys. Res. Lett.*, 32, L08807, doi:10.1029/2004GL022275, 2005

[3] Q. Min, E. Joseph, and M. Duan, "Retrievals of thin cloud optical depth from a multifilter rotating shadowband radiometer", *J. Geophys. Res.*, 109, D02201, doi:10.1029/2003JD003964, 2004

[4] R. Somerville, H. Le Treut, U. Cubasch, Y. Ding, C. Mauritzen, A. Mokssit, T. Peterson, and M. Prather, "Historical Overview of Climate Change", in: *Climate Change 2007: The Physical Science Basis. Contribution of Working Group I to the Fourth Assessment Report of the Intergovernmental Panel on Climate Change,* Solomon, S., D. Qin, M. Manning, Z. Chen, M. Marquis, K.B. Averyt, M. Tignor and H.L. Miller eds., Cambridge University Press, Cambridge, United Kingdom and New York, NY, USA, 2007

[5] B.N. Holben, T.F. Eck, I. Slutsker, D. Tanré, J.P. Buis, A. Setzer, E. Vermote, J.A. Reagan, Y.J. Kaufman, T. Nakajima, F. Lavenu, I. Jankowiak, and A. Smirnov, "Aeronet- a federated instrument network and data archieve for aerosol characterization", *Rem. Sens. Environ.*, 66, pp. 1-19, 1998

[6] A. Smirnov, B.N. Holben, T.F. Eck, O. Dubovik, and I. Slutsker, "Cloud-screening and quality control algorithms for the AERONET database", *Rem. Sens. Environ.*, 73 (3), pp. 337-349, 2000

[7] S. Basart, C. Pérez, E. Cuevas, J. M. Baldasano, and G. P. Gobbi, "Aerosol characterization in Northern Africa, Northeastern Atlantic, Mediterranean Basin and Middle East from direct-sun AERONET Observations", *Atmos. Chem. Phys.*, 9, pp. 8265-8282, 2009

[8] J.G. Chiu, J. C., C.-H. Huang, A. Marshak, I. Slutsker, D. M. Giles, B. N. Holben, Y. Knyazikhin, and W. J. Wiscombe, "Cloud optical depth retrievals from the Aerosol Robotic Network (AERONET) cloud mode observations", *J. Geophys. Res.*, 115, D14202, doi:10.1029/2009JD013121, 2010

[9] L. Alados-Arboledas, H. Lyamani, and F.J. Olmo, "Aerosol size properties at Armilla, Granada (Spain)", *Q. J. R. M. S.*, 129 (590), pp. 1395-1413, 2003

[10] H. Lyamani, F.J. Olmo, A. Alcántara, and L. Alados-Arboledas, "Atmospheric aerosol during the 2003 heat wave in southeastern Spain I: Spectral optical depth", *Atmos. Environ.*, 40, pp. 6453-6464, 2006

[11] M. Shiobara, and S. Asano, "Estimation of cirrus optical thickness from Sun photometer measurements", *J. Appl. Meteorol.*, 33, pp. 672– 681, 1994

[12] B.A. Baum, A.J. Heymsfield, P. Yang, and S.T. Bedka, "Bulk scattering models for the remote sensing of ice clouds. Part 1: Microphysical data and models" *J. Appl. Meteor.*, 44, pp. 1885-1895, 2005

[13] B.A. Baum, and S. Platnick, "Introduction to MODIS cloud products, Earth Science Satellite Remote Sensing, 1: Science and instruments". Edited by J. J. Qu, W. Gao, M. Kafatos, R. E. Murphy, and V. V. Salomonson, Co-published by Tsinghua University Press (Beijing) and Springer-Verlag (Berlin), pp. 74-91, 2006

[14] T. Vincenty, "Direct and Inverse Solutions of Geodesics on the Ellipsoid with application of nested equations", Survey Review XXIII, 176, pp. 88–93, 1975

[15] J.L. Guerrero-Rascado, M.J. Costa, J. Preißler, F. Wagner, and A.M. Silva, "First results about cloud properties obtained by lidar over Évora (Portugal)", in *Book of extended abstracts of Cuarta Reunión Española de Ciencia y Tecnologia de Aerosoles*, pp. C8-1-6, ISBN: 978-84-693-4839-0, 2010

[16] K. Sassen, and J. R. Campbell, "A midlatitude cirrus cloud climatology from the facility for atmospheric remote sensing, part I: macrophysical and synoptic properties", *J. Atmos. Sci.*, 58, pp. 481-496, 2001

[17] J. Reichardt, "Optical and geometrical properties of northern midlatitude cirrus clouds observed with a UV Raman lidar", *Phys. Chem. Earth (B)*, 24, pp. 2555-260, 1999

[18] E. Giannakaki, D. S. Balis, V. Amiridis, and S. Kazadzis, "Optical and geometrical characteristics of cirrus clouds over a Southern European lidar station", *Atmos. Chem. Phys.*, 7, pp. 5519-5530, 2007

[19] S.V. Sunilkumar, K. Parameswaran, and B. V. Krishna Murthy, "Lidar Observations of cirrus cloud near the tropical tropopause: General features", *Atmos. Res.*, 66, pp. 203- 227, 2003

[20] S.V. Sunilkumar, and K. Parameswaran, "Temperature dependence of tropical cirrus properties and radiative effects", *J. Geophys. Res.*, 110, D13205, doi:10.1029/2004JD005426, 2005

[21] S. K. Das, C.-W. Chiang, J.-B. Nee, "Characteristics of cirrus clouds and its radiative properties based on lidar observation over Chung-Li, Taiwan", *Atmos. Res.*, 93, pp. 723–735, 2009